Journal of Alloys and Compounds 489 (2010) 304–309

Contents lists available at ScienceDirect

Journal of Alloys and Compounds

journal homepage: www.elsevier.com/locate/jallcom

The relationship between the g-shift and the local structure for the axial impurity centers in the doped $LiNbO_3$ crystals

T. Bodziony*

Institute of Physics, West Pomeranian University of Technology, Al. Piastow 17, 70-310 Szczecin, Poland

ARTICLE INFO

Article history:
Received 31 July 2009
Received in revised form
14 September 2009
Accepted 15 September 2009
Available online 24 September 2009

PACS:
76.30.−v
76.30.Kg
76.30.Fc

Keywords:
g-Shift method
Superposition model (SPM)
EPR
Lithium niobate
Rare-earth ions
Transitions metal ions

ABSTRACT

The relationship between the g-shift and the local structure of paramagnetic impurity center with axial symmetry is investigated. Spectroscopic data on transitions metal and rare-earth impurities in lithium niobate crystal are used to verify the validity of this method. The distortions around the impurity ions are determined based on the g-shift and compared with experimental data as well as predictions of the superposition model (SPM) and the perturbation methods (PM). The g-shift method yields displacements of impurity ions in good agreement with experimental and SPM or PM predictions. The advantages of the proposed method are discussed.

1. Introduction

The establishment of position of the impurity ions (or defects) in crystals from spectroscopic data is a real problem. The EPR measurements are a sensitive method to detect a local surrounding of the impurity ions [1]. In fact, an impurity ion serves as a probe to study local surrounding. The EPR spectra may indicate a local site symmetry of impurity ions. However it is not easy to extract more detailed structural information from EPR spectra, e.g. lattice distortion around impurity ion. Generally, there are two methods to get this kind of information obtained from spin-Hamiltonian parameters from EPR measurements: (a) superposition model (SPM) [2] and/or (b) perturbation methods (PM) up to second-order (or higher) [3]. SPM serves for modeling of the zero-field splitting (ZFS) parameters or crystal field (CF) ones [2]. The EPR g-parameters ($g_\perp$, $g_{||}$) and hyperfine constants ($A_\perp$, $A_{||}$) are used in PM method [3]. The SPM and PM methods are mathematically sophisticated and practically an advanced programming procedure is necessary to use them.

In this paper we utilize Newman's ideas included in a short paper entitled: "On the g-shift of S-state ions" [4]. He suggested a simple method to extract a structural information from the ZFS parameters (D or b_2^0) and g-shift parameters without using SPM method. It looks strange but we did not find any echoes of this very interesting paper in further investigations since the year 1977. This paper attempts: (1) to recall this paper and (2) to verify and further develop this method by testing it on several ion–host systems. One limitation of this method is, however, that it may be used only for paramagnetic centers with axial symmetry. This paper consists of four sections. In Section 2 the theoretical background of the g-shift method is outlined. The g-shift equation is used and verified in Section 3, where EPR data for different impurities in lithium niobate ($LiNbO_3$) single crystal are analyzed. In Section 4 we provide a short discussion and conclusions.

2. Theoretical background

In general, the spin Hamiltonian (SH) for transitions metal ions (TM) and rare-earth ions (RE) may be written (in the absence of hyperfine structure) as [1,5]:

$$\hat{H} = \mu_B(\vec{B}\cdot\hat{g}\cdot\hat{J}) + \sum_{k,q} B_k^q O_k^q, \quad (1)$$

where O_k^q is a spin operator and J is an angular momentum. Expressions identical with this, except for the replacement of J by S, are

* Tel.: +48 091 449 40 32; fax: +48 091 434 21 13.
E-mail address: tbodziony@ps.pl.

0925-8388/$ – see front matter © 2009 Elsevier B.V. All rights reserved.
doi:10.1016/j.jallcom.2009.09.079

required in Eq. (1) for transition metal ions [1]. The Zeeman term in Eq. (1) for axial symmetry, where the $\boldsymbol{g}$ tensor has two independent components: parallel ($g_{||}$) and perpendicular ($g_{\perp}$) and $g_{||} \neq g_{\perp}$, is given by [1]:

$$\hat{H}_Z = \mu_B[g_{||}B_zJ_z + g_{\perp}(B_xJ_x + B_yJ_y)] \quad (2)$$

Here we consider the question what structural information may be extracted from $g_{||}$ and $g_{\perp}$? One solution was proposed by Newman [4]. We utilize SPM model, which enables to represent g_{ij} factors as summation over contributions from several ligands [4]:

$$\Delta g_{\alpha\beta} = \sum_{ligands\, i} K_{\alpha\beta}(i)\Delta\bar{g}(i) \quad (3)$$

where Δg is the g-shift, $K_{\alpha\beta}(i)$ parameters are determined by the angular coordination of ligands i and $\Delta\bar{g}(i)$ parameter depends only on ligand distance. The transformation properties of $\Delta g_{\alpha\beta}$ give the expressions for $K_{\alpha\beta}(i)$ for a given ligand in terms of its angular position in spherical polar coordinates (θ, φ). Coordination factors $K_{\alpha\beta}$ are given in Appendix A [2,4]. Coordination factors K_2^0 can be simply obtained by the relation [2]:

$$K_2^0[\theta] = \frac{1}{2}(K_{xx} + K_{yy} - 2K_{zz}) = \frac{1}{2}(1 + 3\cos\ 2\theta) \quad (4)$$

according to Ref. [2] (p. 816). The parameter $K_2^0[\theta]$ is function only, one angle θ. Newman focused their analysis of the shift g-shift on the ratio D parameter ($\Delta g/D$) [4]. Here, we consider another aspect. Newman proposed the following formulae defining the normalizing g-shift as a function of θ angle [4]:

$$\frac{g_{\perp} - g_{||}}{g - g_0} = \frac{3}{2}K_2^0[\theta] \cdot n \quad (5)$$

where, $g_0 = 2.0023$ is the free-ion value, $g = (1/3)(2g_{\perp} + g_{||})$ and n is a number of ligands [4]. One can obtain a simple equation connecting the g-shift and the θ angle:

$$\frac{g_{\perp} - g_{||}}{g - g_0} = \frac{3}{4}n(1 + 3\cos\ 2\theta) \quad (6a)$$

or

$$\frac{g_{\perp} - g_{||}}{g - g_0} = \frac{3}{4}n(3\cos^2\ \theta - 1) \quad (6b)$$

One can notice that one polar angle is present in Eqs. (4)–(6). In fact we need only one polar angles to (partially) describe the ion positions in the oxygen octahedron. Let us see on the graphical presentation of the typical oxygen octahedron. Fig. 1 presents a MeO_6 octahedron, where Me-impurity (TM or ER) ion is surrounded by six oxygens. Two angles θ_1 and θ_2 are marked in Fig. 1. First

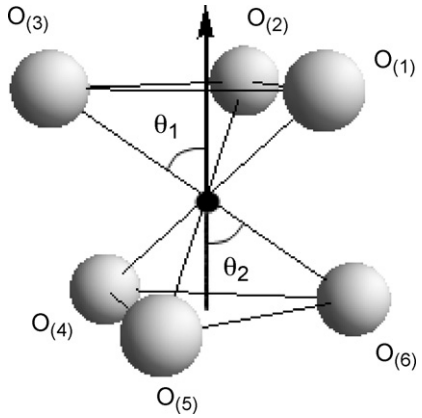

Fig. 1. Oxygen octahedron with marked azimuthally angle.

with oxygens in the "upper" triangle and second with oxygens in the "lower" triangle. The axis symmetry is marked, too.

If the MeO_6 system has cubic symmetry, the Me ion is placed exactly in the middle of the octahedron and $\theta_1 = \theta_2$. If the system has an axial symmetry, Me ion is shifted along the axis symmetry and these angles are different ($\theta_1 \neq \theta_2$). Additionally, if Me ion is moved out of the axis, the MeO_6 system has lower symmetry than axial. One should remember that the angels θ_1, θ_2 are related in the case axial symmetry (see Fig. 1). If we know one angel (e.g. θ_1) for particular MeO_6 system, one can easily establish the second one (e.g. θ_2) based on the crystallographic data. Finally, one can say that one parameter (e.g. the angle θ to the positive axis symmetry (θ_1 in Fig. 1)) describes the position of the impurity ion on the axis symmetry (or oxygen's ions) in oxygen octahedron with axial symmetry. If we know the value of this angle, the position and the displacement of this ion from midway plane can be easily calculated. The establishment of the axis symmetry is very important, too. It can be found on the basis of crystallographic analysis of concrete crystallographic systems. It may be often [1 1 1] axis. One should emphasis that detailed crystallographic analysis is necessary for particularly MeO_6 system to find positions of the Me ion, six oxygen ions, the axis symmetry, angles and so on. Of course, the polar angle θ includes only a part of the structural information about MeO_6 axial symmetry system. We do not say anything about azimuthally angels (φ) or the rotation angle (α) of the lower (and equivalently the upper) triangle of oxygens.

Eq. (6a) or (6b) gives us a simple connection between the g-shift and the polar angle θ, assuming axial symmetry system. On the basis of Eq. (6) one can easily compute the polar angle θ, e.g. the displacements of impurity ion, if the g-shift is known.

3. Comparisons of the experimental and theoretical results

Now let us compare results arising from Eq. (6) with experimental results and those obtained theoretically by SPM or PM methods. We investigate a lithium niobate crystal (LN, $LiNbO_3$). Lithium niobate single crystals doped by very wide range of elements in various concentrations were investigated in different methods for many years. There are many papers about LN doped with transitions metal (TM) ions: Mn^{2+}, Fe^{3+}, Cr^{3+} or rare-earth ions (RE^{3+}) like: Er^{3+}, Yb^{3+}, Nd^{3+}. We concentrate on these impurities in LN single crystal, in which there are results of computed displacements of impurity ions and which were found by us.

The lithium niobate (LN, $LiNbO_3$) is a ferroelectric crystal having useful dielectric elastic and optoelectronic properties [6]. The properties and applications of LN crystal have been widely studied for many years. The structure of the $LiNbO_3$ has been studied by Abrahams et al. [7,8]. The Curie temperature of lithium niobate is $T_c = 1190\,^{\circ}C$ [6]. The LN crystal is rhombohedral belonging to the space group $R3c$ ($C_{3v}{}^6$) at room temperature. The unit cell dimensions are $a = 5.14739(8)$ Å and $c = 13.85614(9)$ Å [7,8]. The chains of LiO_6 an NbO_6 octahedrons along the C_3 axis being the crystallographic and the optical axis c-axis (or z) are important part of the LN structure. The sequence of octahedrons repeats as {Li, Nb, vacancy, etc.}. These chains are connected to each other by oxygen bridge [7,8]. Fig. 2 shows a structure of LiO_6 an NbO_6 octahedrons in LN crystal. The Li^+ and Nb^{5+} ions are surrounded by six oxygen atoms arranged in distorted octahedron but away from its center [8]. It is found that the distance Li–O is equal to 2.2711(7) and 2.0050(3) Å, where as corresponding angles are $\theta = 43.97^{\circ}$ and 70.78°, respectively, in LiO_6 octahedron. The distance Nb–O is equal to 2.1296(9) and 1.8763(7) Å, where as corresponding angles are $\theta = 47.76^{\circ}$ and 62.10°, respectively, in NbO_6 octahedron (see Fig. 2) [8]. The schematic view of the Li and Nb octahedrons stacked along the trigonal axis (C_3) are presented in Fig. 3. The oxygen's octahedron is shown in Fig. 3. The δ_{Li} and δ_{Nb} are the distance (or

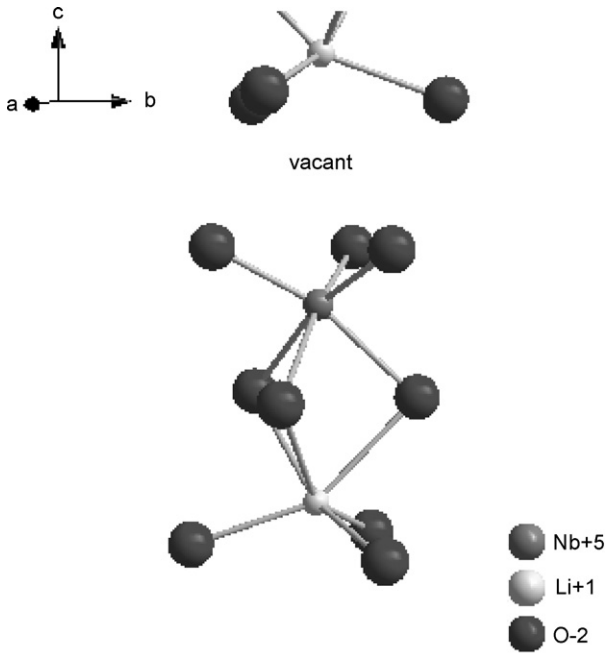

Fig. 2. The structure of LiO_6 an NbO_6 octahedrons along the c (C_3) axis in $LiNbO_3$ crystal.

displacements) of cations, Li^+ and Nb^{5+}, respectively, to midway planes marked by dashed lines. Transition ions (TM) or rare-earth ions (RE) in ferroelectric $LiNbO_3$ can enter any of the three possible sites: Li^+, Nb^{5+}, and structural vacancy site [6]. Our analysis will concentrate to paramagnetic centers assuming that TM and RE ions substitute Li^+ or Nb^{5+} site.

3.1. Neodymium centers in lithium niobate crystals

There are several papers about neodymium doped $LiNbO_3$:Nd crystal. Choh et al. [9] report SH parameters of new Nd^{3+} (and Er^{3+}) centers in lithium niobate single crystal. The EPR g-factor and the local structure for the trigonal Nd^{3+} center in $LiNbO_3$:Nd single crystal are investigated, too [10]. Wu and Dong used the perturbation theory of the EPR g factors ($g_\perp$ and $g_{||}$) and established an off-center displacement Nd^{3+} ions from Li^+ site [10]. The results are gathered in Table 1. Displacement δ means a dislocation of Nd^{3+} (Nd_{Li}) impurity from Li^+ site in LiO_6 octahedron (see Fig. 4) obtained based on Eq. (6a). The values of the displacements δ obtained from other methods are revealed in Table 1, too.

Table 1
EPR g factors and displacement of the Nd^{3+} centers at Li^+ site in $LiNbO_3$:Nd single crystal.

$g_{||}$	$g_\perp$	Displacement, δ (Å)	Temperature
1.43(2)	2.95(5)	−0.25(3)	4 K [9]
1.315(2)	3.012(5)	−0.37(3) ÷ −0.28[a], −0.4[b]	20 K [10,11]

[a] Calculated on PM method [10].
[b] Measured from RBS spectrometry [12].

Wu and Dong (PM method) estimated an off-center displacement as equal to −0.28 Å [10]. The displacement obtained from Rutherford backscattering spectrometry (RBS) experiment is equal to −0.40 Å [12]. One can notice that better agreement with RBS result was obtained using our method (−0.37 Å versus −0.28 Å in comparison to −0.40 Å). The displacement of Nd_{Li} impurity decreases with the decrease of temperature (see Table 1). Fig. 4 presents schematic view of the local structure of the trigonal Nd_{Li} center in $LiNbO_3$ crystal. The Nd^{3+} ion replacing the Li^+ ion undergoes an off-center displacement δ away from the center of oxygen octahedron along C_3 (z or c) axis.

Finally, one can emphasis a very good agreement between displacement of Nd^{3+} ion calculated form Eq. (6) and those obtained from PM theory [10] and, especially, with RBS experiment [12] in the case of $LiNbO_3$:Nd single crystal.

3.2. Erbium centers in lithium niobate crystals

The Er^{3+} paramagnetic centers with axial symmetry in $LiNbO_3$ single crystals were investigated by many scientists [3,9,13,14]. We are focused on the Er^{3+} centers in $LiNbO_3$ and MgO or ZnO codoped $LiNbO_3$ crystals because one can compare our results with those obtained by other methods in the case of this crystal. The results of

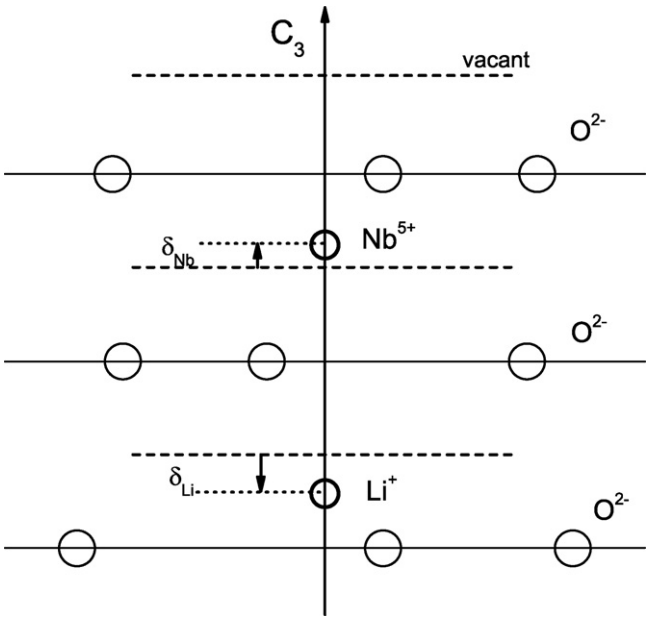

Fig. 3. Schematic view of the LiO_6 an NbO_6 octahedrons along the trigonal (C_3 or c) axis in $LiNbO_3$ crystal.

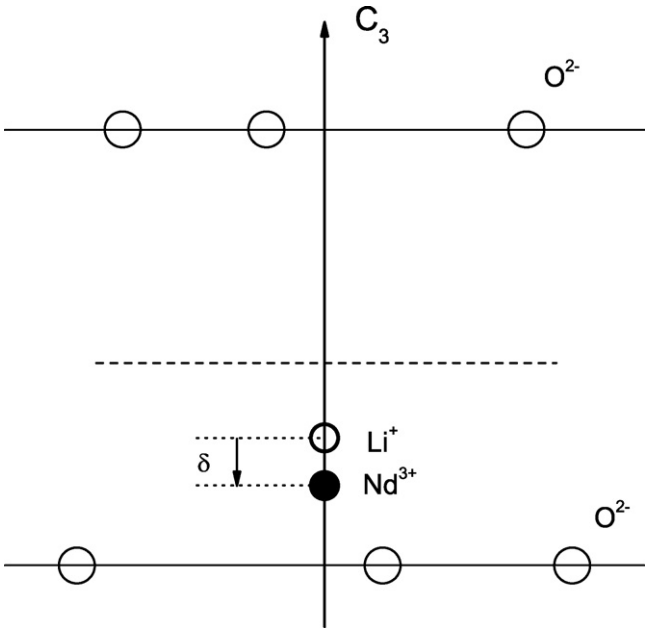

Fig. 4. Schematic view of the local structure of the axial (trigonal) Nd^{3+} center in $LiNbO_3$:Nd single crystal with marked displacements of Nd^{3+} ion from Li^+ site.

Table 2
EPR g-factors and displacement of the trigonal Er^{3+} centers in $LiNbO_3$:Er and MgO or ZnO codoped crystals.

$g_{\|\|}$	$g_\perp$	Displacement, δ (Å) at		Compound
		Nb^{5+} site	Li^+ site	
4.3(2)	7.6(3)	−0.17(1) ÷ 0.39[a]	−0.10(1) ÷ 0.30[a], −0.2[b]	LN:Er, MgO [13,14]
4.26(5)	7.8(1)	−0.17(1) ÷ 0.39[a]	−0.11(1) ÷ 0.30[a], −0.2[b]	LN:Er, ZnO [13,14]

[a] Calculated on PM method [3].
[b] Measured from RBS spectrometry [12].

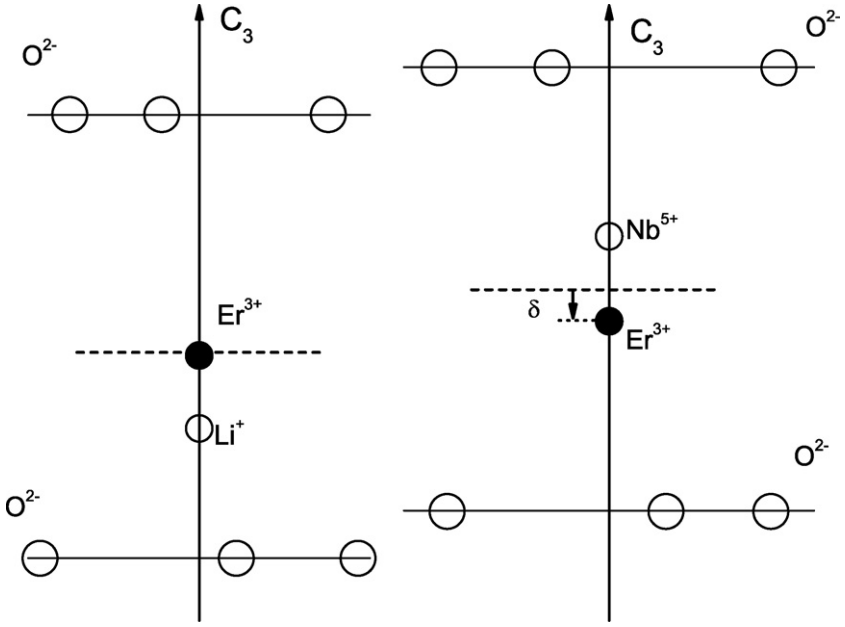

Fig. 5. Schematic view of the local structure of the axial (trigonal) Er^{3+} center in MgO codoped $LiNbO_3$:Er single crystal at Li^+ site (left picture) and Nb^{5+} site (right picture).

theoretical studies of the EPR g-parameters and defect structures of trigonal Er^{3+} centers in $LiNbO_3$ and MgO or ZnO codoped $LiNbO_3$ crystals were presented [3]. The Er^{3+} ions may occupy Nb^{5+} site or Li^+ site in LN crystal [3,13,14]. The perturbation formula of EPR g factors ($g_{||}$, $g_\perp$) was established and the results of displacements of Er^{3+} centers from center of the oxygen octahedron were published [3]. The authors [3] report that Er^{3+} do not occupy exactly the Li^+ and Nb^{5+} site, but are displaced along C_3 axis away from the center of oxygen octahedron by about 0.39 Å for Er_{Li} center and towards the center of octahedron by about 0.30 Å for center Er_{Nb}. The results of using Eq. (6) to Er_{Li} and Er_{Nb} centers are presented in Table 2. Displacement δ means a dislocation of Er^{3+} impurity from the center of oxygen octahedron.

Fig. 5 shows the schematic view of the local structure of the trigonal Er^{3+} center in MgO codoped $LiNbO_3$:Er single crystal at Li^{5+} site (left picture) and Nb^{5+} site (right picture). A similar picture can be obtained for ZnO codoped $LiNbO_3$:Er single crystal (see the value of displacements in Table 2).

The displacement of the Er^{3+} from Li^+ site (Er_{Li} center) obtained from X-ray standing way (XSW) is equal to $\delta \cong -0.46$ Å [15] and measured by RBS/channeling technique $\delta \cong -0.2$ Å [12]. Unfortunately, no experimental results for Er^{3+} displacement from Nb^{5+} site (Er_{Nb} center) in LN crystal are available [3]. Comparing the displacement of Er^{3+} centers computed using Eq. (6) ($\delta \cong -0.1$ Å and $\delta \cong -0.2$ Å) PM method ($\delta \cong -0.39$ Å, $\delta \cong -0.30$ Å [3] for Er_{Li} and Er_{Nb} center, respectively) and finally those measured from experimental method (possibly only for Er_{Li} center, $\delta \cong -0.2$ Å [12]) one can see that we obtain a very good agreement with correct sign, better than those from PM method. Additionally, one may note that the value of the displacement of Er_{Li} center is small. It means that the Er^{3+} ion is placed close to the middle of the oxygen octahedron (see Fig. 5, left picture). Assuming that Er^{3+} ions substitute Li^+ site and simultaneously Nb^{5+} site is vacant (V_{Nb}), one can observe that oxygen ions "above" and "below" Er_{Li} center will be connected with the Er^{3+} in the same manner (see Fig. 3). Besides dislocation of Er_{Li} center towards the center of the octahedron, one can expect a move of oxygen ions. Finally, it may happen that Er^{3+} ion locates in the center of the octahedron yielding $g_{||} \cong g_\perp$ and for cubic Er^{3+} center in $LiNbO_3$:Er single crystal [16]. The charge compensation in doped lithium niobate can be achieved in congruent $LiNbO_3$ in different ways, for example by Li^+ or Nb^{5+} vacancies in various positions [17].

3.3. Chromium centers in lithium niobate crystals

Now let us consider a chromium (Cr^{3+}) center with axial symmetry in $LiNbO_3$:Cr single crystals [18,19]. The results of displacements of the Cr^{3+} impurity from the center of oxygen octahedron assuming that Cr^{3+} ion enters Li^+ or Nb^{5+} sites are listed in Table 3. Table 3 shows that the displacement of the Cr_{Li} and Cr_{Nb} centers from the center of oxygen octahedron is approximately equal in both cases and equals $\delta \cong -0.3$ Å. The electron nuclear double resonance (ENDOR) measurements suggested that if Cr^{3+} ion substitutes Nb^{5+}, it is displaced towards the center of oxygen octahedron by about 0.12 Å [3].

Table 3
EPR g-factors and displacement of the trigonal Cr^{3+} centers in $LiNbO_3$:Cr crystals.

$g_{\|\|}$	$g_\perp$	Displacement, δ (Å)			Reference
1.969	3.870	−0.26	–	Li^+ site	[18,19]
1.969	3.870	−0.34	0.12[a]	Nb^{5+} site	[18,19]

[a] From ENDOR measurement [3].

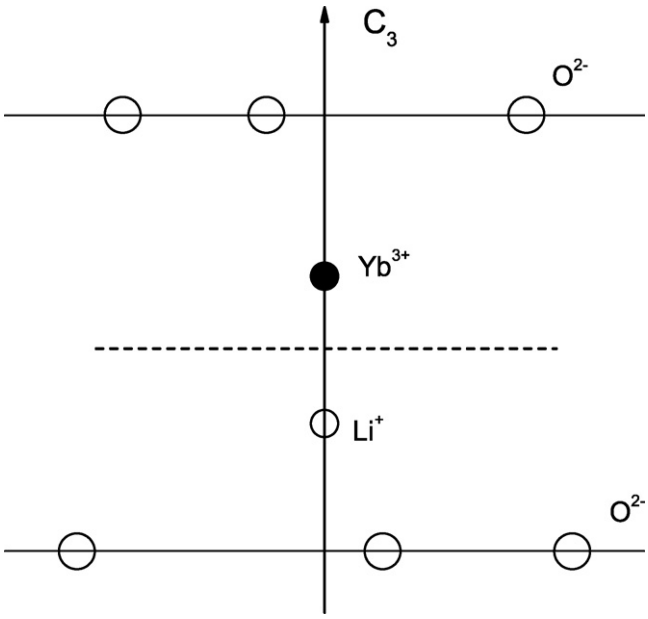

Fig. 6. Schematic view of the local structure of the axial Yb^{3+} center in $LiNbO_3$:Yb single assuming that Yb^{3+} ion substitutes Li^+ site.

One can conclude that the displacement for Cr_{Nb} center obtained from Eq. (6) (see Table 3) is comparable with experimental results. The displacements of the impurity ions may be influenced by the temperature.

3.4. Ytterbium centers in lithium niobate crystals

The Yb^{3+} paramagnetic centers in $LiNbO_3$ and Mg:$LiNbO_3$ single crystals were investigated by Bonardi et al. [20]. They found a new axial Yb^{3+} center ($g_{||} = 4.70 \pm 0.03$ and $g_{\perp} = 2.70 \pm 0.02$), which was attributed to Yb^{3+} ion at the Li^+ site [20]. Yb^{3+} ion is displaced along C_3 axis towards the center of the octahedron by about 0.78 Å from the Li^+ position (0.3 Å from the center of oxygen octahedron, see Fig. 3). Fig. 6 shows LiO_6 octahedron with marked Yb^{3+} ion position.

Table 4
EPR g-factors and displacement of the Fe^{3+} and Mn^{2+} axial centers in $LiNbO_3$:Fe, $LiNbO_3$:Mn crystals, respectively.

$g_{||}$	$g_{\perp}$	Displacement, δ (Å)		Reference
1.984(3)	1.992(3)	0.15(2)	Fe^{3+} at Li^+ site	$LiNbO_3$:Fe [21]
1.984(3)	1.992(3)	0.10(2)	Fe^{3+} at Nb^{5+} site	$LiNbO_3$:Fe [21]
2.019	1.983	–	Fe^{3+} at Li^+ or Nb^{5+} site	$LiNbO_3$:Fe [23]
1.997(3)	2.009(1)	−1.3(9)	Mn^{2+} at Li^+ site	$LiNbO_3$:Mn [22]
1.997(3)	2.009(1)	−1.4(9)	Mn^{2+} at Nb^{5+} site	$LiNbO_3$:Mn [22]

The Rutherford backscattering (RBS channeling) spectrometry reveals that Yb^{3+} ion is shifted away from the Li^+ position by about −0.3 Å [12]. Our result seems closer to the measured value but of opposite sign

3.5. Fe^{3+} and Mn^{2+} centers in lithium niobate crystals

We are focused on analyzing ^6S state Fe^{3+} [21] and Mn^{2+} [22] ions in $LiNbO_3$. The results of calculation using the superposition model (SPM) for zero-field splitting parameters (ZFS) b_2^0, b_4^0, b_4^3 and b_4^{-3} for both above centers in lithium niobate crystals are presented in Refs. [21,22]. Additionally we analyze other axial Fe^{3+} center in $LiNbO_3$:Fe reported by Malovitchko et al. [23].

The results of using the Newman equation (Eq. (6)) for these paramagnetic centers are gathered in Table 4. Displacement δ means dislocations Fe^{3+} and Mn^{2+} impurity from the center of oxygen octahedron. The first and second rows of Table 4 show the axial Fe^{3+} center measured for Fe^{3+} (0.01 wt.%) doped $LiNbO_3$ single crystal at room temperature [21]. Fig. 7 presents the schematic view of the local structure of this Fe^{3+} center at the Li^+ site (left picture) and Nb^{5+} site (right picture). The deformation of the oxygen octahedron is smaller, if Fe^{3+} ion substitute Nb^{5+} site. It suggests that Fe^{3+} ion may easily substitute Nb^{5+} site then Li^+ site. Our result is consistent with results obtained by Yeom et al. [21].

The analysis of Mn^{2+} centers in LN:Mn crystal shows a wide range of displacement δ (see last two rows of Table 4). The distance between the center of the oxygen octahedron (a midway plane) and the planes of oxygen is about ~1.2 Å. It is easy to see that Mn^{2+} ion (or Fe^{3+} ion [23]) may be out of oxygen octahedron!

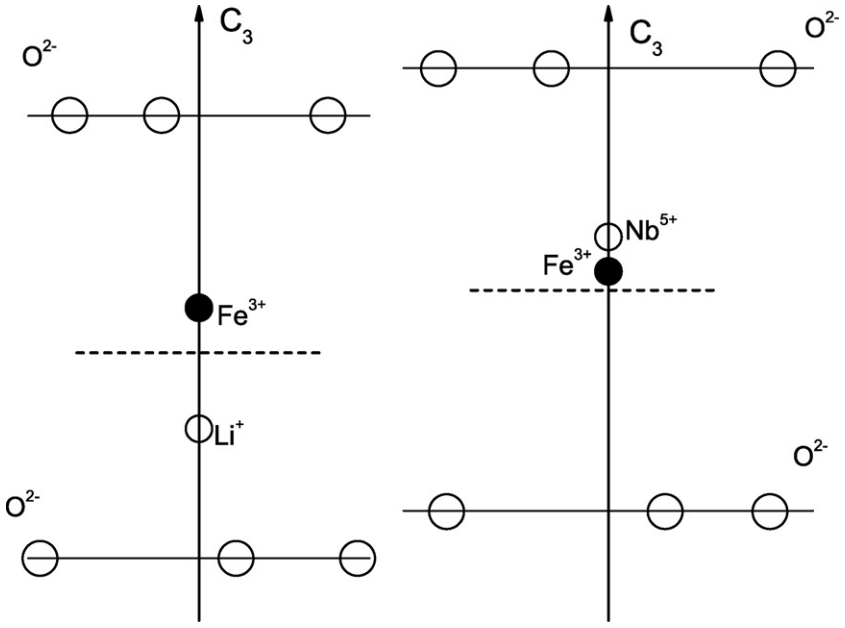

Fig. 7. Schematic view of the local structure of the axial Fe^{3+} center at Li^+ site (left picture) and Nb^{5+} site (right picture) in $LiNbO_3$:Fe single crystal.

Therefore we should study only the low limit of the displacement, which is equal to −0.4 and −0.5 Å assuming Mn^{2+} at Li^{+} site and Mn^{2+} at Nb^{5+} site, respectively ($LiNbO_3$:Mn crystal [22]). V.K. Jain published in 1992 the superposition model analysis of zero-field splitting (b_2^0 parameter) of Mn^{2+} center in $LiNbO_3$ crystal [24]. The estimated displacements of Mn^{2+} ion at Li^{+} and Nb^{5+} site are equal to 0.3 and 0.5 Å, respectively [22,24]. The low limit of displacements of Mn^{2+} at Li^{+} site and Mn^{2+} at Nb^{5+} seem quite similar to those obtained from papers [22,24]. However, an error analysis (and common sense) is indispensable. If the errors of $g_{||}$ and $g_{\perp}$ are not given, we may be unable to estimate the displacement of impurity ion based on Eq. (6) (position of the impurity ion may be out of the octahedron, see middle row in Table 4 [23]).

4. Discussion and conclusions

The discussion and conclusions will be presented in a few short points.

(1) The g-shift analysis and Newman equation (Eq. (6)) may give us structural information about paramagnetic systems with axial symmetry.
(2) The correctness of g-shift analysis and Newman equation was tested on several impurities in lithium niobate crystal (see: Nd^{3+} center in $LiNbO_3$:Nd, Er^{3+} centers in $LiNbO_3$:Er, MgO, Cr^{3+} centers in $LiNbO_3$:Cr, Yb^{3+} centers in $LiNbO_3$:Yb^{3+}, Fe^{3+} and Mn^{2+} centers in $LiNbO_3$:Fe, $LiNbO_3$:Mn crystals).
(3) The comparison of the computed displacements of impurity ions with experimental or those established on the basis of SPM or PM methods shows that our results stay in good or even very good agreement both in S-state ions (Fe^{3+} and Mn^{2+}) and the other RE and TM ions (Nd^{3+}, Er^{3+}, Yb^{3+}, Cr^{3+}).
(4) This method failed only in one example, in which g-factors were given without errors (see Table 4). The error analysis (and common sense) may be indispensable.
(5) The g-shift method enables to partial structural information about paramagnetic systems. We may establish a polar angle (θ) and distance between impurity ion and oxygen ligands. We do not say anything about azimuthal angels (φ) or the rotation angle (α) of the lower (and equivalently the upper) triangle of oxygen's. The full information may be obtained only using SPM or PM procedures.
(6) We can acquire a similar information using SPM or PM procedures. Nevertheless SPM or PM methods are much more complicated. The proposed method is simple and quick.
(7) When we are using SPM or PM procedure, it is very important to choose correctly a starting value of the angles (θ_i, φ_i) and distances R_i. The angles and distances (θ_i, R_i) computed based on the g-shift method can be used as starting point in SPM or PM procedures.
(8) Using g-shift method (and similarly SPM or PM procedure) must be followed by detailed crystallographic analysis.

The g-shift method was verified on a several paramagnetic centers in lithium niobate single crystal. This method should be tested on other paramagnetic centers with axial symmetry and the results must be verified experimentally by EPR and theoretically by SPM (and/or) PM methods. However, the preliminary results on LN crystal seem attractive. It appears that some useful information about the substitutional positions for paramagnetic impurity centers with axial symmetry can be easily obtained by analyzing the g-shift parameters.

Acknowledgement

This work was partially supported by the research grant from the Polish Ministry of Science and Tertiary Education in the years 2006–2009.

Appendix A. Coordination factors

Coordination factors $K_{\alpha\beta}$ are given by equations [2]:

$$\begin{aligned} K_{zz}[\theta] &= \sin^2\theta \\ K_{xx}[\theta,\varphi] &= 1-\sin^2\theta\cos^2\varphi \\ K_{yy}[\theta,\varphi] &= 1-\sin^2\theta\sin^2\varphi \end{aligned} \tag{A.1}$$

and

$$\begin{aligned} K_{xy}[\theta,\varphi] &= K_{yx}[\theta,\varphi] = -\sin^2\theta\sin\varphi\cos\varphi \\ K_{zx}[\theta,\varphi] &= K_{xz}[\theta,\varphi] = -\frac{1}{2}\sin 2\theta\cos\varphi \\ K_{zy}[\theta,\varphi] &= K_{yz}[\theta,\varphi] = -\frac{1}{2}\sin 2\theta\sin\varphi \end{aligned} \tag{A.2}$$

References

[1] A. Abragam, B. Bleaney, Electron Paramagnetic Resonance of Transition Ions, Clarendon Press, Oxford, 1970.
[2] D.J. Newman, W. Urban, Adv. Phys. 24 (1975) 793.
[3] S.-Y. Wu, W.-C. Zheng, Phys. Rev. B 65 (2002) 224107.
[4] D.J. Newman, J. Phys. C: Solid State Phys. 10 (1977) L315.
[5] C. Rudowicz, Magn. Reson. Rev. 13 (1987) 1.
[6] Properties of Lithium niobate, EMIS Datarevies, Series No. 5, 1989.
[7] S.C. Abrahams, J.M. Reddy, J.L. Bernstein, J. Phys. Chem. Solids 27 (1966) 997.
[8] S.C. Abrahams, P. Marsh, Acta Crystallogr. B 42 (1986) 61.
[9] S.H. Choh, J.H. Kim, I.-W. Park, H.J. Kim, D. Choi, S.S. Kim, Appl. Magn. Reson. 24 (2003) 313.
[10] S.-Y. Wu, H.-N. Dong, J. Alloys Compd. 386 (2005) 52.
[11] R. Jablonski, I. Pracka, M. Swirkowicz, SPIEE 3178 (1997) 303.
[12] J. Garcia Sole, L.E. Bausa, D. Jaque, E. Montoya, H. Murrieta, E. Jaque, Spectrochim. Acta Part A 54 (1998) 1571.
[13] D.M.B.P. Milori, I.J. Moraes, A.C. Hernandez, R.R. de Souza, SiuF L.M., M.C. Terrile, Phys. Rev. B 51 (1995) 3206.
[14] D. Bravo, A. Martin, F.J. Lopez, Solid State Commun. 112 (1999) 541.
[15] T. Gog, M. Griebienow, G. Materlik, Phys. Lett. A 181 (1993) 417.
[16] T. Bodziony, Opt. Mater. 31 (2008) 149.
[17] J. Diaz-Caro, J. Garcia-Sole, D. Bravo, J.A. Sanz-Garcia, F.J. Lopez, F. Jaque, Phys. Rev. B 54 (1996) 13042.
[18] T.H. Yeom, Y.M. Chang, C. Rudowicz, S.H. Choh, Solid State Commun. 87 (3) (1993) 245.
[19] G. Burns, D.F. O'Kane, R.S. Title, Phys. Rev. B 167 (1969) 314.
[20] C. Bonardi, C.J. Magon, E.A. Vidoto, M.C. Terrile, L.E. Bausa, E. Montoya, D. Bravo, A. Martin, F. Lopez, J. Alloys Compd. 323–324 (2001) 340.
[21] T.H. Yeom, S.H. Choh, C. Rudowicz, Phys. Status Solidi (b) 185 (1994) 409.
[22] T.H. Yeom, S.H. Choh, C. Rudowicz, Phys. Status Solidi (b) 185 (1994) 417.
[23] G.I. Malovichko, V.G. Gratchev, O.F. Schrimer, B. Faust, J. Phys.: Condens. Matter 5 (1993) 3971.
[24] V.K. Jain, Solid State Commun. 84 (6) (1992) 669.